AL48 - Impact of Anode Change on MHD in Aluminum Reduction Cell

Zhibin Zhao[1,*], Wei Liu[2] ,Qinsong Zhang[3], Xi Cao[4], Junfeng Qi[5] and Michael Ren[6]
1.Chief Engineer
2. Director
5. Research Engineer
Science and Technology Management Department, Shenyang Aluminium& Magnesium Engineering & Research Institute Co., Ltd., Shenyang, China
3. Chief Engineer
4. Engineer
Aluminum Reduction Department, Shenyang Aluminium& Magnesium Engineering & Research Institute Co., Ltd., Shenyang, China
6. Managing Director,
Sunlightmetal Consulting Inc. Toronto, Canada
Corresponding author: zhibin.zhao@sami.com.cn

Abstract

Anode change is one of the most important operations in modern aluminum electrolysis industry. The impact of new anodes on the pot primarily focuses on two aspects: the thermal component and the magnetohydrodynamic (MHD) component. Our previous [1] paper discussed the thermal impact by anode changing. This study now shifts our focus to explore the MHD impact of the anode change.

It is found that the anode-cathode distance (ACD) would be squeezed if the total voltage of the cell remained unchanged during anode change. An increase of pot voltage is required to maintain its original ACD. We delved into the consequences of anode change on various aspects through numerical simulations and industrial measurements. This paper also delves deeper into understanding the underlying mechanism behind “sensitive anodes”, by exploring horizontal current redistribution, metal flow pattern and magnitude, and interface deformation after anode change.

Some potential methods to mitigate the impact of anode change are explored here. Optimizing the operations of anode change and implementing the "customized technology for anode set modifier" are short-term endeavors, while selecting a suitable anode set modifier may require a longer-term effort.

Keywords: Aluminum reduction cell, Anode change, MHD stability.

1. Introduction

Since its invention, the technology and design of the Hall-Héroult reduction cell have undergone significant advancements, with cell capacity increasing from 4 kA to 600 kA and current efficiency increasing from 75 % to 96 %. Despite these substantial developments, the Hall-Héroult reduction cell remains the sole primary aluminum smelting process utilized commercially.

Anode change or anode replacement is the most important routine practice in modern aluminum electrolysis industry. The anode is consumed at a rate of about 1.5-1.8 cm per day, proportional to current density. When the anode reaches the end of its service life, the anode butt is replaced by a new anode. The impact of new anodes on the pot primarily focuses on two aspects: the thermal component and the MHD component.

The first aspect concerns the thermal balance. Introducing cold anodes could have a significant impact on the thermal equilibrium of aluminum reduction pots. In our previous paper [1], we examined the thermal effects resulting from anode changes. The theoretical calculations of heat absorption and generation revealed that the commonly used anode set modifier in most aluminum smelters is insufficient to maintain its own thermal balance after an anode change.

Another crucial aspect to consider is the MHD balance. In the process of aluminum reduction, direct current is supplied to the electrical layers of the bath and metal, both of which exist within a magnetic field environment. The magnetic field is also generated inside and outside of the pot by its high electric current. The effect of magnetic field and direct current in an electrical fluid conductor can lead to MHD-related issues. During the practice of anode change, the just set new anodes are wrapped by a layer of insulating solidified electrolyte, which impedes the current flow in the anode and generates large horizontal current in the aluminum pad. It is well-known that a significant horizontal current can have adverse effects on the MHD balance.

This paper serves as a continuation of our previous discussion regarding the thermal impact of anode change in aluminum reduction cells. However, this study will now shift its focus to explore the MHD impact of anode change. We conducted theoretical calculations and analyses concerning the changes in ACD after anode replacement.

Through numerical simulations (ANSYS and CFX) and industrial measurements, we delved into the consequences of anode change on various aspects. These included the influence on the horizontal current in the metal pad, alterations in the flow pattern and magnitude of metal velocity, as well as the deformation of the bath-metal interface. Our findings provide insights into the MHD effects resulting from anode replacement in aluminum reduction cells.

2. Theoretical Analysis

We selected a 500 kA cell with 48 anodes as our physical geometry. The anodes size and other physical parameters were used to analyze the theoretical calculations of ACD change during anode changing.

2.1 Geometry, Simplifications or Assumptions

Figure 1 illustrates the schematic diagram of a modern Hall-Héroult reduction cell. For better understanding of the problem discussed here, only the anode assembly and bath in the blue box are considered.

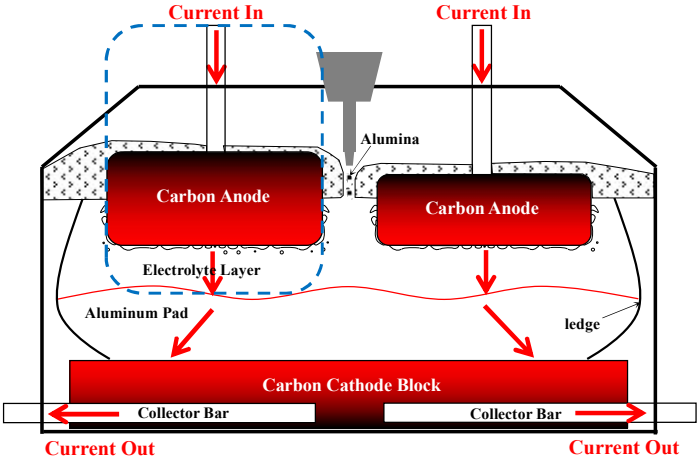

Figure 1. Schematic diagram of a typical Hall-Héroult reduction cell.

Based on the number of anodes, this blue box segment can be divided into 48 parallel circuits, as illustrated in Figure 2. Each section's resistance within the blue box can be represented by Equation (1). The voltage drop can be calculated accordingly by the similar equation.

$$R = R\_rod + R\_stub + R\_cast\_iron + R\_contact + R\_anode + R\_bubble + R\_Bemf + R\_bath \quad (1)$$

in which

R_rod	Resistance of anode rod;
R_stub	Resistance of stub;
R_cast_iron	Resistance of cast iron;
$R\_contact$	Contact resistance of cast iron and anode carbon;
R_anode	Resistance of anode carbon;
R_bubble	Resistance of anodic bubbles;
R_Bemf	Equivalent resistance of reversible potential plus over voltages;
R_bath	Ohmic resistance of bath.

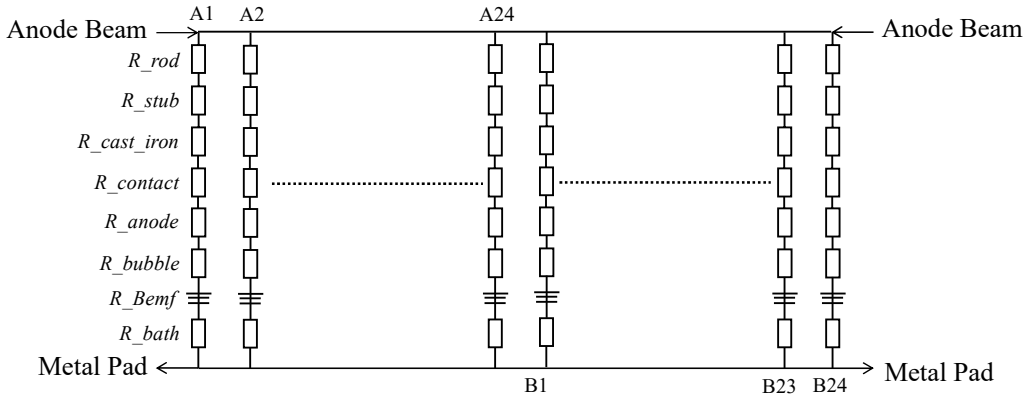

Figure 2. Simplified equivalent circuit of anode assembly and bath.

As the real electric behavior in commercial cells is coupled with complex phenomena including current distribution, chemical reaction, thermal and mass transport, some simplifications or assumptions were also made to focus only on the electric flow:

1. The influence of current density variation during anode changing on reversible potential and over voltages was not considered;
2. The resistivity of anode carbon, bath, cast iron, stub and rod were set as fixed values, which means the electrical resistivity change caused by temperature was ignored in this work;
3. The resistivity of electrolyte is 100 times that of anode carbon (4.50×10^{-3} Ω·m for electrolyte and 4.50×10^{-05} μΩ·m for anode), it was assumed that the current flowed vertically downwards into electrolyte layer. There was no horizontal current flow in the electrolyte layer;
4. The influence of transient interface deformation of metal/bath was not considered.

Based on the aforementioned simplifications or assumptions, the exact extent of the impact remains uncertain. However, through qualitative, semi-quantitative, and even quantitative analysis, we can obtain some insights into the MHD impact. We will continue to incorporate the aforementioned assumptions into our calculations in the future.

Three cases were carried out using the geometries shown in Figure 3, where the grayscale represented different anode consumption heights. Case 1 is a normal production case in aluminum reduction cell, it also can be set as base case; Case 2 is to simulate the routine practice of two

anodes change (A1A2); Case 3 represents an abnormal situation of four anodes change (A1A2+A11A12), which may occur in early operation period.

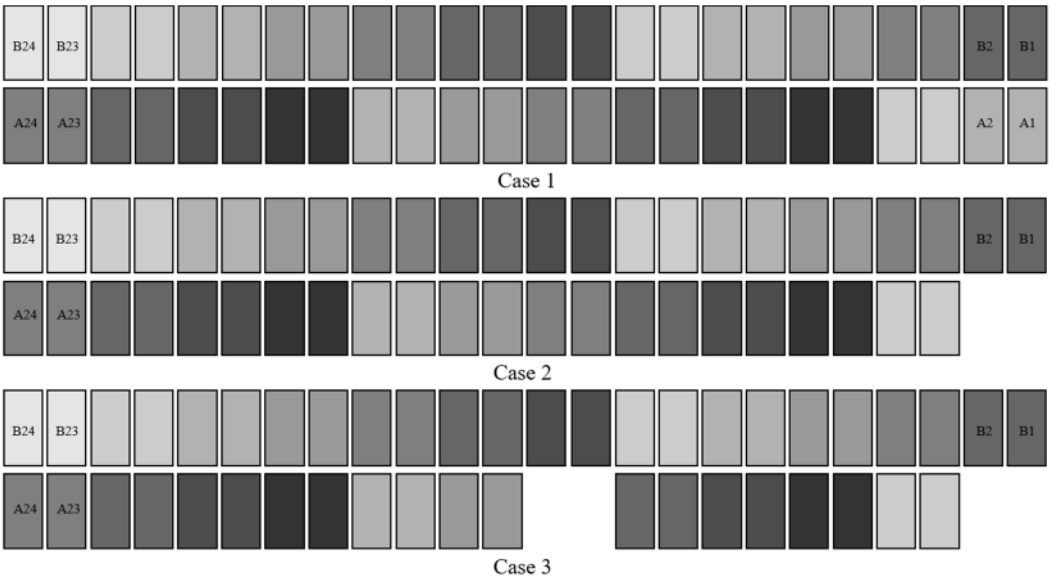

Figure 3. Geometries of three cases conducted here (Grayscale representing different anode heights).

2.2 Calculations and Analysis

In Figure 2, *V_rod, V_stub* and *V_cast_iron* are chosen as 0.025 V, 0.050 V, and 0.007 V respectively based on previous numerical simulations [2] and industrial measurements [3]. *V_contact* is set as 0.082 V based on data from reference [4]. It was reported that the bubble coverage of 36-77 % [5] and thickness of 5 mm [5] results in an extra voltage drop of about 0.150 to 0.350 V [6]. Then the *V_bubble* is taken as 0.250 V here. The ACD is set as typical, 0.045 m, and the voltage drop of bath is calculated based on the resistivity and geometry in Figure 3 as 1.616 V.

Due to the continuous consumption of anodes, the anodes in the production electrolytic cell are distributed at different heights, as shown in Figure 3. The total resistance of the anode carbon in this case with different heights is calculated by Equation (2), which is 2.6 x 10^{-07} ohm. The voltage drop of anode carbon for the 500 kA cell is found to be 0.129 V.

$$1/R = \frac{1}{R_{A1}} + \frac{1}{R_{A2}} + \frac{1}{R_{A3}} + \ldots\ldots\ldots\ldots \frac{1}{R_{B24}} \qquad (2)$$

The above component voltage drops represented in Figure 2 are listed in Table 1. The total voltage drop is 2.159 V. In this section, the voltage drop of the other two cases is also set as 2.159 V.

Table 1. Partial voltage drop in Figure 2.

Parts	Case 1	Case 2	Case 3
V_rod (V)	0.050	0.052	0.054
V_stub (V)	0.007	0.007	0.007
V_cast_iron (V)	0.025	0.026	0.027
V_contact (V)	0.082	0.085	0.089

V_anode (V)	0.129	0.140	0.153
V_bubble (V)	0.250	0.261	0.273
V_Bath (V)	1.616	1.588	1.555
ACD (m)	0.045	0.042	0.040

Case 2 is to simulate the routine practice of two anodes change. When new anodes are set into the bath, a large amount of heat is extracted from the bath and transferred into heating the new cold anodes, freezing the surrounding bath. The conductivity nature of new anodes is extremely poor, even the current tends towards to zero. In this case, we believe that only 46 anodes share the total current of 500 kA for a period of time after anode change. The total resistance of the anode carbon in this case is calculated by Equation (3), which is 2.8×10^{-07} Ω. The voltage drop of anode carbon increases to 0.140 V.

$$1/R = \frac{1}{R_{A3}} + \ldots\ldots\ldots\ldots \frac{1}{R_{B24}} \quad (3)$$

In this case, the number of conductive anode rods decreases from 48 to 46, and the resistance or voltage drop of rods are slightly increased to 0.052 V based on equation (4).

$$V\_rod = V\_rod \times 48/46 \quad (4)$$

Similarly, *V_stub, V_cast_iron, V_contact* and *V_bubble* are also slightly increased, shown in Table 1. The calculation method is the same as equation (4).

Based on assumption (1), there is no change on *V_ Bemf* .

Assuming that the total voltage (anode assembly and bath) remains unchanged during anode change, the voltage drop of bath decreases from 1.616 V to 1.587 V. Based on assumption (3), the conductive area of electrolyte layer is also decreased by 2/48 after anode change. It can be calculated that ACD in this case is 0.042 m, which is reduced by about 3 mm compared to the case before anode change.

It is necessary to increase the pot voltage by 0.113 V to maintain the same ACD as before the anode change like Case 2. In some extreme circumstances listed in Case 3, the pot voltage increase needs to go up to 0.194 V to maintain its original ACD.

Table 2 lists three kinds of anode set modifiers applied in SY500 kA smelters, in which the same pot design and capacity were applied. In Smelter A, the initial anode set modifier is to increase the pot voltage by +45 mV for 40 minutes in the first stage, then decrease to +30 mV for 40 minutes in the second stage, and finally decrease to +15 mV for 40 minutes. Smelter B and Smelter C have similar strategies, but the detailed values are different.

The current and geometry calculated here are the same as our previous calculations [1]. In which, the anode set modifier is not sufficient to support thermal balance during anode change. From the perspective of MHD balance in this section, the anode set modifier is also not enough to compensate the decrease of ACD after anode change.

Taking Smelter A as an example, the biggest modifier is +45 mV, which illustrates that the ACD is squeezed by about 2.1 mm after the anode change.

Table 2. Anode set modifier in different smelters.

Smelter A		Smelter B		Smelter C	
magnitude (mV)	duration (min)	magnitude (mV)	duration (min)	magnitude (mV)	duration (min)
45	40	75	45	90	60
30	40	50	45	60	60
15	40	25	45	30	60

3. Numerical Analysis

3.1 Horizontal Current in Metal Pad

In previous research and cell design, our focus has primarily been on the horizontal current in the width direction of the aluminum liquid [7-8]. However, the considerable horizontal current generated in the length direction during anode change has been largely overlooked.

Following the replacement of an anode, it temporarily becomes non-conductive or conducts only a minimal amount of current for a certain period of time. Because the conductivity of the aluminum liquid is about 10 000 times of the bath, a significant horizontal current will be formed in the region near the anode change. Figure 4 is a vector diagram of ANSYS simulation results of horizontal current in aluminum liquid. A normal case (before change), a case of internal anode change (A11A12) and a case of corner anode change (A1A2) are shown.

Changing the internal anodes leads to significant alterations in the horizontal current, which differ from the case with no anode change or the condition before the anode replacement. The horizontal current mainly comes from the surrounding adjacent and opposite anodes, and it increases more sharply as it is closer to the new anodes. The value of horizontal current is greater by to 2 to 3 times than that of no anode change case. This situation is even worse in the case with corner anode change. The horizontal current is clearly larger than that of internal anode change case.

To provide a clearer understanding of the size and distribution of the horizontal current, Figure 5 illustrates the distribution of each horizontal current interval in various cases. The horizontal current magnitude along the length direction is mainly concentrated between -100 A/m^2 and 100 A/m^2 before anode change, and it is basically symmetrically distributed (Figure 5a). The proportion of current in this range is up to 78 %. Figure 5b displays the horizontal current distribution in the case with internal anode change. The current is mainly distributed between - 4000 A/m^2 and 4000 A/m^2. The proportion is about 77 %. Furthermore, it is evident that there is a substantial horizontal current with values reaching up to 8000 A/m^2. The proportion in this part is 14 %. Figure 5c illustrates the distribution of the horizontal current when the corner anode is changed. The most obvious phenomenon is the current bias, which is mainly distributed from -8000 A/m^2 to 0. In this case, the proportion of horizontal current exceeding 8000 A/m^2 increases to 25 %.

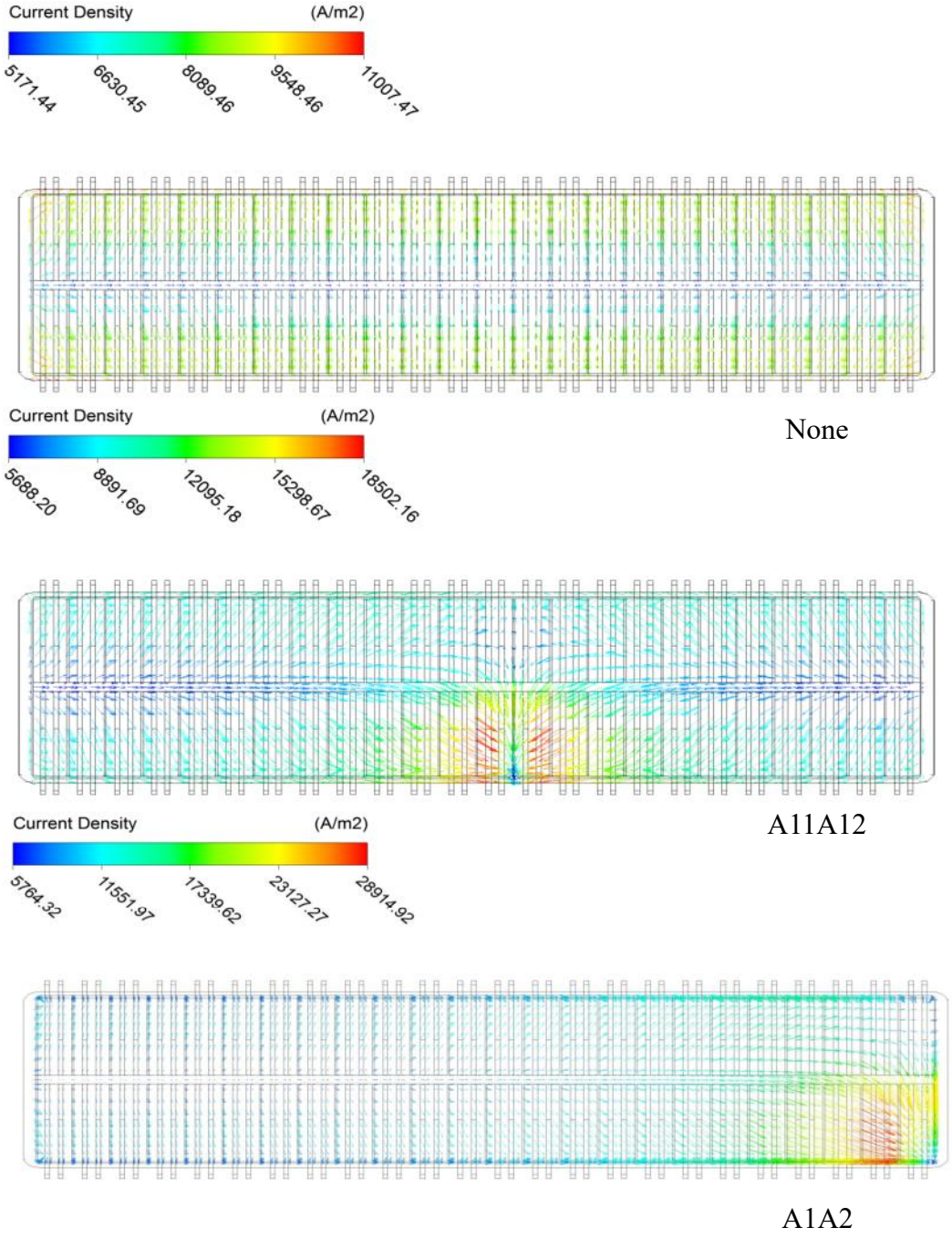

Figure 4. Horizontal current in metal pad before and after anode change.

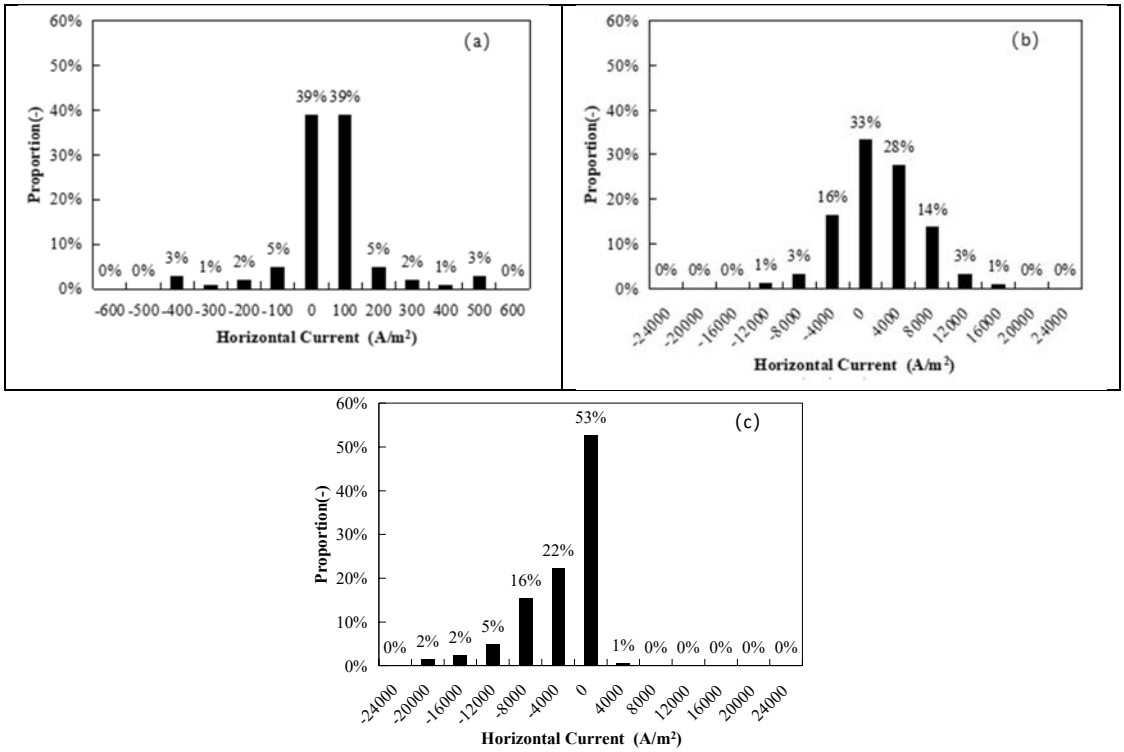

Figure 5. Distribution of horizontal current before and after anode change.

3.2 Flow Pattern and Velocity Magnitude of Metal Pad

The increase of horizontal current causes the change of the electromagnetic force, which will directly affect the velocity of metal flow. Figure 6 shows the flow pattern and velocity magnitude of liquid aluminum before and after anode change. Commercial software CFX was used here.

All cases show a similar pattern. The flow field presents two different size vortexes. The vortex close to the duct end flows counterclockwise, occupying a larger region (anode 11 to anode 24). On the other hand, the vortex close to the tap end flows clockwise and covers a smaller area of anode 1 to anode 10. The velocity of all cases is basically in the same magnitude range. The area with the larger velocity is distributed near the anode A3 to anode A7, anode A14 to anode A23.

While the flow pattern and velocity magnitude exhibit similar characteristics in all three cases, there are also some subtle differences that can be observed. Anode A11 and anode A12 are internal anodes and located on the edge of two vortexes. Due to the horizontal current beneath new anodes, there are two small vortexes here. In the case of corner anode change, there is no clear vortexes beneath new anodes, but the velocity near new anodes (anode A3 to anode A7) is clearly increased.

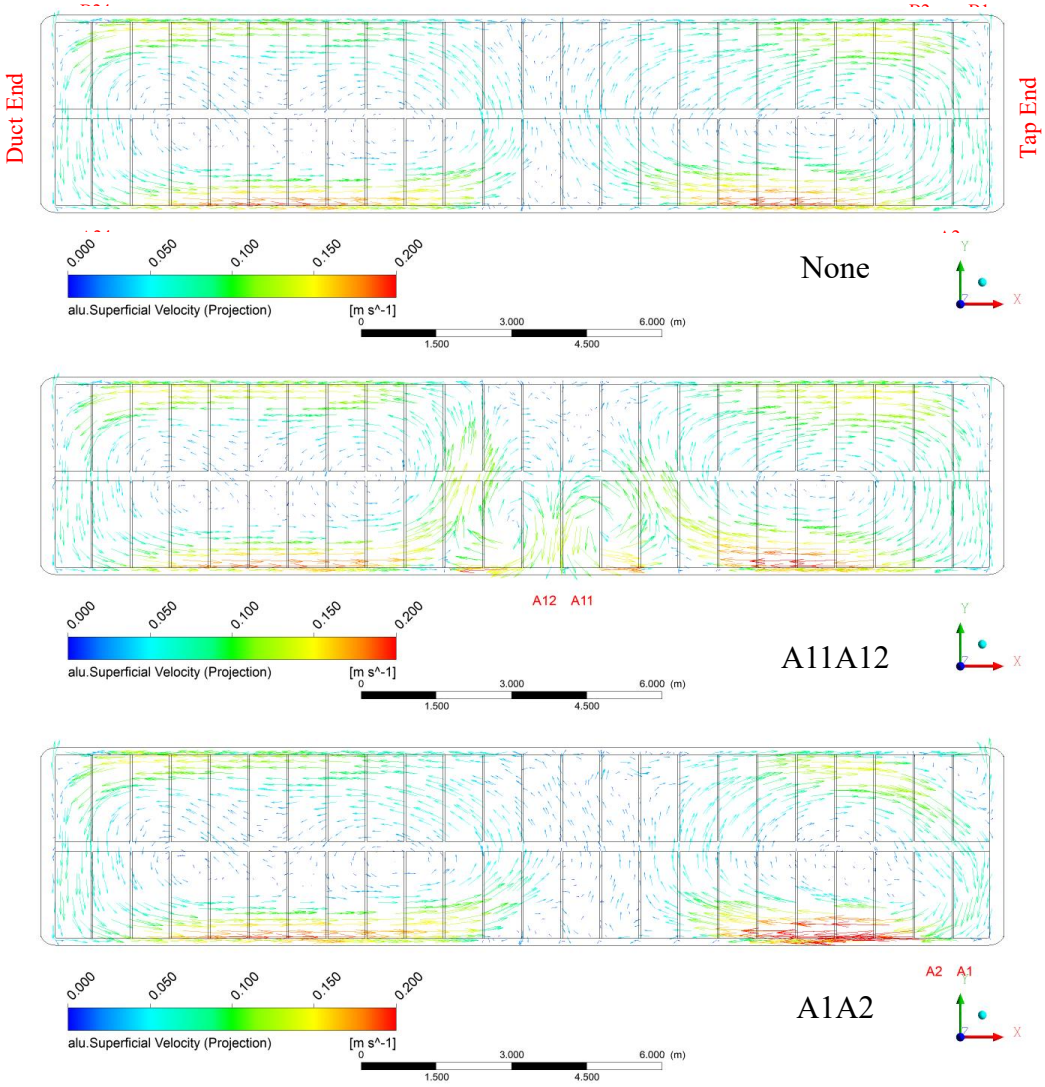

Figure 6. Flow pattern and velocity magnitude before and after anode change.

3.3. Metal/Bath Interface Deformation

The increase in horizontal current leads to changes in the electromagnetic force, directly impacting the interface deformation of the metal and bath. Figure 7 presents the simulation results of liquid metal interface shape.

In the case with no anode change, the interface deformation ranges from -35 mm to 31 mm. The total deformation amplitude is 66 mm. The upward deformation region is primarily concentrated at the duct end and tap end. Conversely, the downward deformation is distributed along the anode riser busbar side (also called side A).

In the case of internal anode change, the interface deformation ranges from -37 mm to 33 mm. The deformation amplitude increases to 70 mm. The upward deformation beneath new anodes is larger than that of base case. Our primary focus lies on the upward deformation rather than the downward deformation. From the perspective of maintaining ACD here, during anode change, the pot voltage should increase by approximately 0.076 V to compensate for the needed increase of 2 mm of ACD.

The interface deformation range of corner anode change is from -36 mm to 40 mm. The deformation amplitude increases to 76 mm, which is clearly larger than that of internal anode case and the base case. The most upward deformation area is mainly located beneath the new anode A1 and A2. The pot voltage should increase about at least 0.323 V during the corner anode change to compensate for the needed increase of ACD.

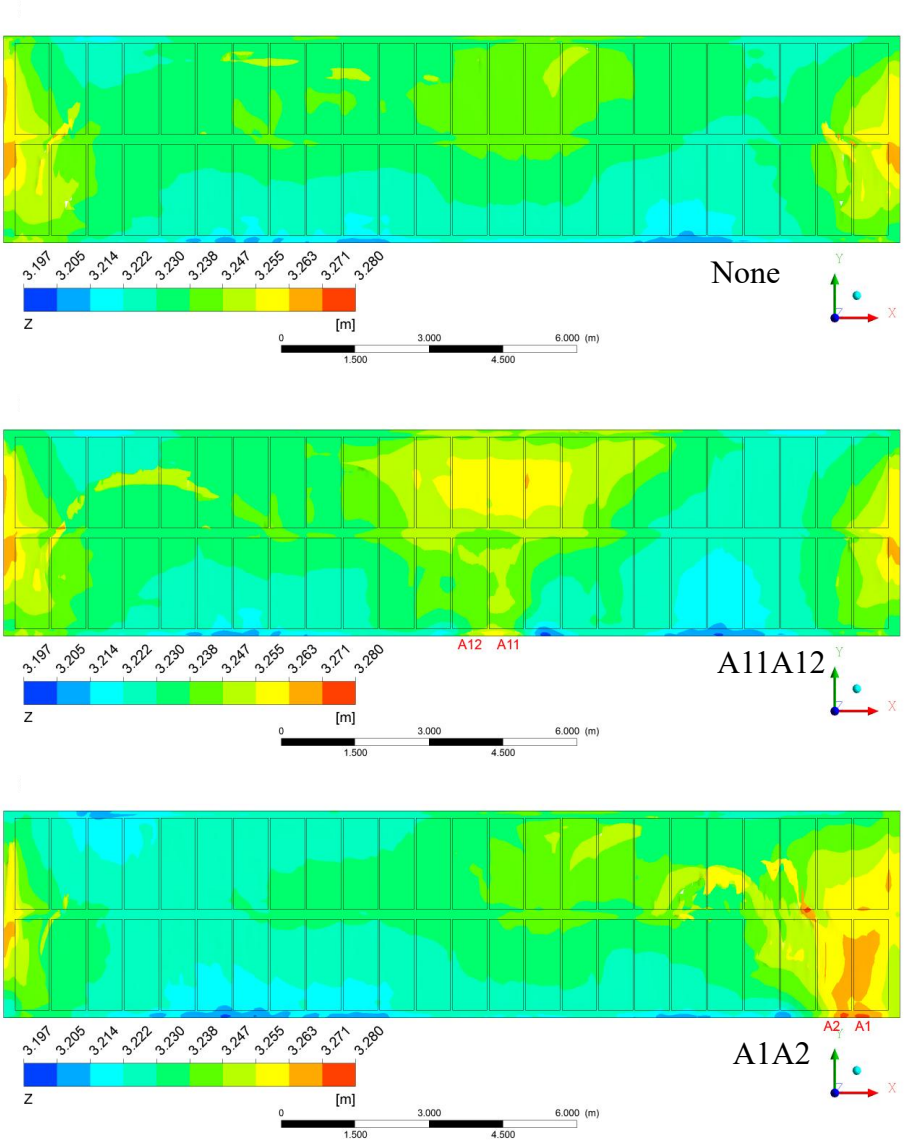

Figure 7. Metal/Bath interface deformation before and after anode change.

To further analyze the impact of anode change on the interface deformation, Figure 8 shows the comparisons of deformation degrees. In the range with interface deformation exceeding 30 mm, there is only 0.2 % to 0.4 % for the three cases. In the range with interface deformation over 20 mm, the proportion before anode change is 3.7 %, and it is increased to 5.2 % for internal anode change and 8.5 % for corner change respectively. The proportion of deformations above 20 mm in the corner anode change is 2.3 times that of before anode change. The proportion of interface deformation over 10 mm before anode change is 34.4 %, and this proportion increased to 41.9 % and 51.0 % respectively after anode change.

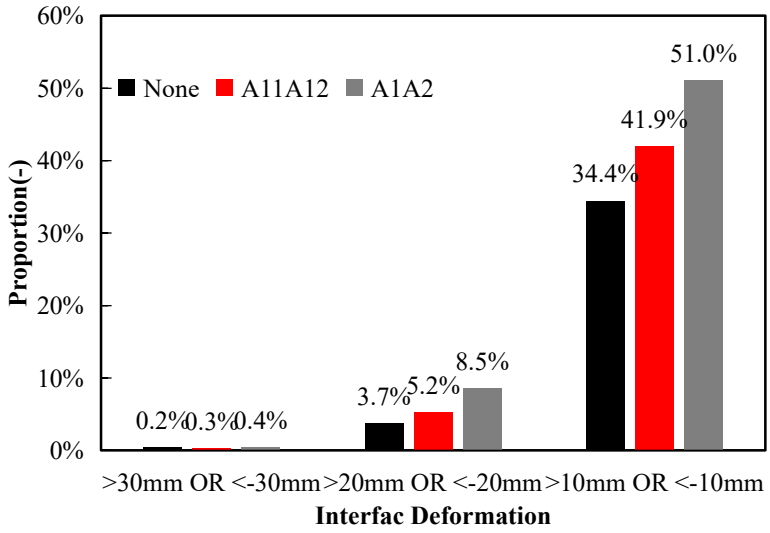

Figure 8. Proportion comparison of different amplitudes of interface deformation.

Due to the upwards trend after anode change, we summarized the probability of abnormal voltage fluctuation after anode change in real cells shown in Figure 9 [9]. After anode change, the average probability of abnormal fluctuations is approximately 27 %. However, specific unreasonably high probabilities are notably observed at A21, A22, A23, and A24. The findings from Figure 7 and Figure 8 help explain this phenomenon. The interface beneath new anodes presents an upward deformation trend both in the cases of corner anodes and of internal anodes, which means that the local ACD is squeezed. This trend is more obvious in the case of corner anodes. With the same anode set modifier, the local ACD near corner anodes is smaller than that of internal anodes after change, increasing the possibility of connection of anode bottom and metal variation peak.

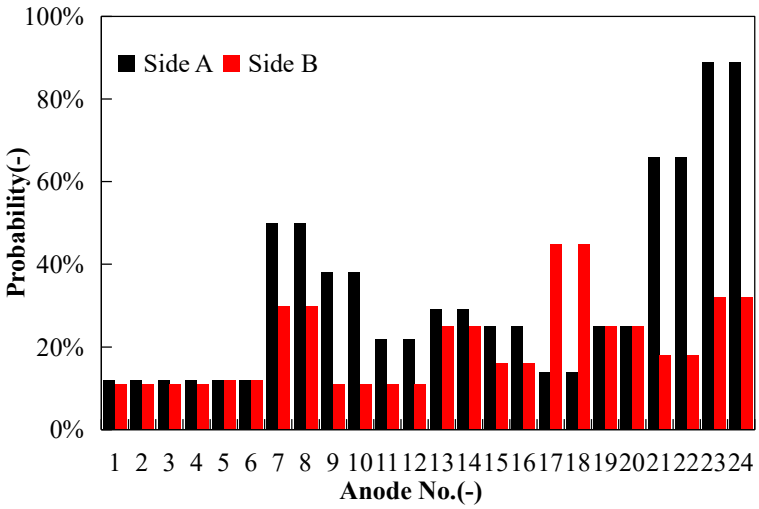

Figure 9. Probability of abnormal voltage fluctuation after anode change.

4. Discussion

In the production practice, new anodes typically require approximately 24 hours to draw full current. However, it is quite common for the recovery time of the new anode current to exceed 24 hours, sometimes extending up to 48 hours. Figure 10 shows an example of current pick up at different times after anode change. The current pick up rate of new anodes is only slightly above 50 % after 23 hours, and it takes about 43 hours to reach full current.

The anode current profile represents the ACD distribution [10]. If the recovery of new anode current is too slow, it is difficult for the interface deformation to return to its original state before anode change. The abnormal voltage fluctuation described in Figure 9 is also easy to occur. The key to solving this problem is to decrease the impact of anode change, and increase the anode current pick up rate.

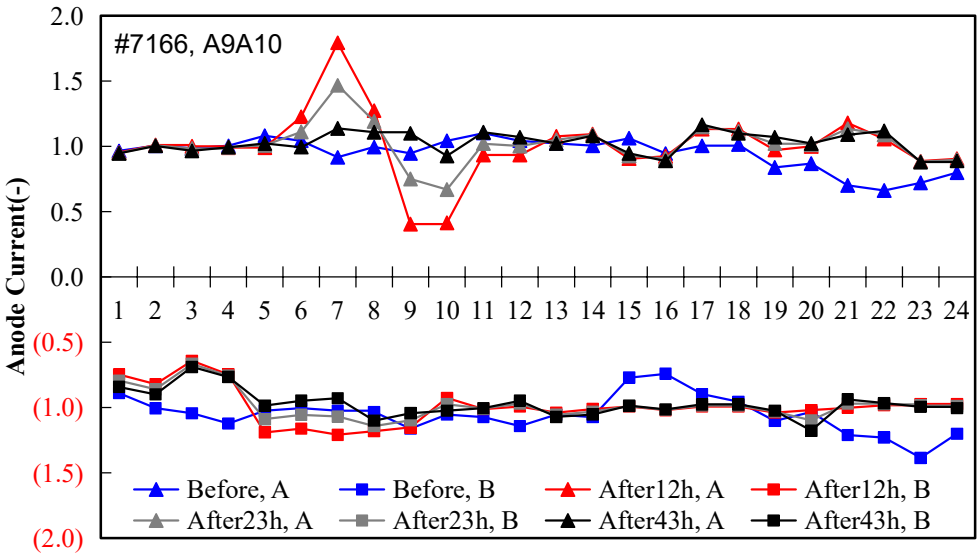

Figure 10 Anode current profile before and after anode change.

4.1 Anode Set Modifier

In industrial practice, anode set modifiers are commonly applied during anode change to enhance heat generation and to maintain ACD.

In our previous calculations [1], when the anode set modifier was applied, it resulted in a reduction of 4.8 °C in the bath and metal temperature. Additionally, a 1 cm increase of side ledge thickness was assumed. Despite these adjustments, there remains a 49 % deficiency in heat or energy for one anode change. To ensure that a reasonable ACD is maintained, an anode set modifier of at least 0.113 V is required for the pot to increase by approximately 3 mm in ACD after anode change. From both the thermal and MHD perspectives, a larger anode set modifier is essential to achieve this goal.

Given that the anode set modifier is applied to the entire cell, the sudden increase in heat input could potentially ruin the thermal balance of the test pots. Therefore, the exact magnitude and duration of the modifier should be chosen with great caution and careful consideration. Recently, some scholars have started investigating the anode change process by coupling multi-field and bath solidification and melting [11-13], which has yielded valuable results. The combination of numerical simulation with industrial testing to select an appropriate modifier could be an effective approach. However, it may be a long-term work.

4.2 Operations

Selecting the right anode set modifier may indeed be a long-term process; however, optimizing the operations of anode change can lead to significant benefits and rewards.

Following anode change, a potential operational approach could involve reducing or temporarily

shutting down alumina feeding in the region of newly changed anodes. Simultaneously, the deficiency of alumina can be compensated for by adjusting the feeding points nearby. For instance, the first feeding point of total 6 feeders could be shut down during 3 hours after A1A2 change, and feeding point 2 and 3 compensate alumina at a rate of 1.4 or 1.5 times of their original feeding. This approach not only reduces energy absorption in the new anode area, but also accelerates the consumption of alumina in the covering material that falls into the bath during anode change.

The anode current online monitoring system should be installed on the reduction cells. The operators should pay close attention to the current pick up rate of new anodes. When it is detected that the recovery rate of the new anode current is abnormal, some adjustments should be made accordingly.

Anode change is a manual operation and is subject to human influence. Strengthening the training of workers is a rapid way to enhance the quality of anode change. This includes effectively cleaning impurities, crust pieces, and cover material pieces that may fall into the bath. Additionally, setting the appropriate height of new anodes, improving anode quality, and reducing carbon dust are all essential measures to be implemented.

4.3 Customized Technology for Anode Set Modifier

Both thermal and MHD impacts of anode change in aluminum reduction cell show that anode change in a pot has an individual characteristic. There are some "sensitive anodes" with larger possibility of abnormal voltage fluctuation, more obvious upward metal deformation trend, and smaller anode current pick up rate.

To address the issue of "sensitive anodes," a "customized technology for anode set modifier" was proposed [1], specifically tailored for various anode change scenarios. Both numerical and industrial work has proven that this technology played a positive role in improving thermal and electrical behavior of "sensitive anodes" without any thermal and MHD issues.

5. Conclusions

This paper combines theoretical calculations, numerical simulations, and statistical results from industrial measurements to analyze the MHD impact of anode change in aluminum reduction cells.

Theoretical calculation and analysis of ACD change after anode change were conducted. With the total voltage drop of the cell (represented by anode assembly and bath) remaining unchanged during anode change, the ACD is squeezed from 45 to 42 mm. To maintain its original ACD, an increase of pot voltage by 0.113 V is required.

Our previous work [1] identified certain “sensitive anodes” characterized by a lower anode current pick up rate. This paper delves deeper into understanding the underlying mechanism behind this phenomenon, exploring horizontal current redistribution, metal flow pattern and magnitude, and interface deformation after anode change.

This paper also explores potential methods to mitigate the impact of anode change. Optimizing the operations of anode change and implementing the "customized technology for anode set modifier" are short-term endeavors, while selecting a suitable anode set modifier may require a longer-term effort.

6. References

1. Zhibin Zhao, Wei Liu, Yafeng Liu, Michael Ren, and Zhaowen Wang, A discussion on

thermal impact of anode change in aluminum reduction cell [J]. *Light Metals* 2023, 128-136.
2. Fuqiang Wang, Xi Cao, Qinsong Zhang, Yafeng Liu, Xiaodong Yang, and Dongfang Zhou, Numerical simulation research and application of electric-thermo-stress coupled field for anode assembly [J]. *Light Metals* 2019 (5), 22-25 (In Chinese).
3. SAMI. Physical field measurements of aluminum reduction cell - electric field part [R]. *Internal Report* 2019 (In Chinese).
4. Tuofu Li. Numerical simulation study on optimization of anode structure of aluminum reduction cell for energy saving [D]. *Northeastern University,* Shenyang, China 2020.
5. Zhibin Zhao, Zhaowen Wang, Bingliang Gao, Yuqing Feng, Zhongning Shi, and Xianwei Hu, Anodic bubble behavior and voltage drop in a laboratory transparent aluminium electrolysis cell [J], *Metallurgical and Materials Transactions B* 2016 47(3), 1962-1975.
6. Warren E. Haupin, A scanning reference electrode for voltage contours in aluminum smelting cells [J], *Journal of Metals* 1971 (10), 46-49.
7. Xiaodong Yang, and Wei Liu, Discussion on designing high amperage energy saving aluminum reduction pot - busbar, cathode structure and MHD stability [J], *Light Metals* 2016 (10), 27-32. (In Chinese)
8. Wei Liu, Dongfang Zhou, Yafeng Liu, Ming Liu, and Xiaodong Yang. Simulation and measurements of the flow filed of 600 kA aluminum reduction pot [J], *Light Metals* 2015, 497-482.
9. Xi Cao, Qinsong Zhang, Zhibin Zhao, Yafeng Liu, Hongwu Hu, Zhe Dong, and Haigang Wu, Study on the rule of interfacial deformation and anode current distribution evolution of aluminium reduction cell during anode changing [J]. *Light Metals* 2021 (06), 20-28 (In Chinese).
10. Fuqiang Wang, Zhaowen Wang, Qinsong Zhang, Zhibin Zhao, Shaohu Tao, Wei Liu, and Xiaodong Yang. Computation and validation of ACD for aluminum reduction cell [J]. *Light Metals* 2022 (02), 23-25 (In Chinese).
11. Qiang Wang, Baokuan Li, and Mario Fafard, Effect of anode change on heat transfer and magneto-hydrodynamic flow in aluminum reduction cell, *JOM* 2016 (68), 610-622.
12. Zhibin Zhao, Wei Liu, and Yafeng Liu. Numerical study and industrial testing on optimizing new anode behavior by changing additional voltage strategies [C], *Proceedings of 38th International ICSOBA Conference*, Virtual, 16-18 November, 2020, Papre AL13, Travaux 49, 679-689.
13. Hongliang Zhang, Qiyu Wang, Shuai Yang, Jie Li, Jinding Liang, and Ling Ran, Numerical investigation of flow field effect on ledge shape in aluminum reduction cell by coupled thermo-flow model [J], *Light Metals* 2020, 517-526.